Published in final edited form as:
Biochemistry. 2013 December 31; 52(52): 9413–9425. doi:10.1021/bi4010304.

Lack of synchronization between iron uptake and cell growth leads to iron overload in *Saccharomyces cerevisiae* during post-exponential growth modes

Jinkyu Park[†], **Sean P. McCormick**[†], **Mrinmoy Chakrabarti**[†], and **Paul A. Lindahl**[†,‡,*]

[†]Department of Chemistry, Texas A&M University, College Station, Texas 77843-3255, United States

[‡]Department of Biochemistry and Biophysics, Texas A&M University, College Station, Texas 77843-2128, United States

Abstract

Fermenting cells growing exponentially on rich (YPAD) medium transitioned to a slow-growing state as glucose levels declined and their metabolism shifted to respiration. During exponential growth, Fe import and cell growth rates were matched, affording an approximately invariant cellular Fe concentration. During the transitionary period, the high-affinity Fe import rate declined slower than the cell growth rate declined, causing Fe to accumulate, initially as Fe^{III} oxyhydroxide nanoparticles but eventually as mitochondrial and vacuolar Fe. Once in slow-growth mode, Fe import and cell growth rates were again matched, and the cellular Fe concentration was again approximately invariant. Fermenting cells grown on minimal medium (MM) grew more slowly during exponential phase and transitioned to a true stationary state as glucose levels declined. The Fe concentration of MM cells that just entered stationary state was similar to that of YPAD cells, but MM cells continued to accumulate Fe in stationary state. Fe initially accumulated as nanoparticles and high-spin Fe^{II} species, but vacuolar Fe^{III} also eventually accumulated. Surprisingly, Fe-packed 5-day-old MM cells suffered no more ROS damage than younger cells, suggesting that Fe concentration alone does not accurately predict the extent of ROS damage. The mode and rate of growth at the time of harvesting dramatically affected cellular Fe content. A mathematical model of Fe metabolism in a growing cell was developed. The model included Fe import via a regulated high-affinity pathway and an unregulated low-affinity pathway. Fe import from the cytosol into vacuoles and mitochondria, and nanoparticle formation were also included. The model captured essential trafficking behavior, demonstrating that cells regulate Fe import in accordance with their overall growth rate and that they misregulate Fe import when nanoparticles accumulate. The lack of regulation of Fe in yeast is perhaps unique compared to the tight regulation of other cellular metabolites. This phenomenon likely derives from the unique chemistry associated with Fe nanoparticle formation.

Iron plays fundamental roles in enzyme catalysis, electron transfer processes, small-molecule binding and activation. This redox-active transition metal is found in various forms, including Fe/S clusters (ISCs), heme centers, nonheme mono- and dinuclear

[*]Corresponding Author: Phone: 979-845-0956. Fax: 979-845-4719. Lindahl@chem.tamu.edu.

Note: The authors declare no competing financial interest.

Supporting Information. Figure S1, Fet3p expression levels in cells harvested at different time points; Figure S2, chronological profile of Zn concentrations in cell for 5 days; Figure S3, 100 K MB spectrum of 5-day MM-grown cells; Figure S4, MB spectrum of mitochondria isolated from 5-day MM-grown cells; Figure S5, loading controls for Western blots; Figure S6, ODEs for version *V*; Table S1, and Mösbauer parameters determined from the spectra in the main text. This material is available free of charge via the Internet http://pubs.acs.org.

complexes, among others. Fe can also be deleterious to cells, as certain forms participate in Fenton chemistry that generates ROS which can, in turn, damage DNA, proteins, and membranes.[1] Like all cellular processes, Fe trafficking and metabolism are commonly considered to be tightly regulated.

The molecular-level details of Fe trafficking and regulation are best understood in the budding yeast *Saccharomyces cerevisiae*. Major "traffic hubs" in Fe metabolism include mitochondria and vacuoles, but the plasma membrane, cytosol and nucleus also play important roles.[2,3] The plasma membrane contains numerous proteins that import Fe from the environment. The membrane-bound Fet3p/Ftr1p complex constitutes the "high affinity" Fe importer.[4] Genes encoding these and about 20 other Fe-related proteins are controlled by Aft1p/Aft2p.[5] These transcription factors are sensitive (via a partially understood mechanism) to the concentration of unidentified Fe-containing species in the cytosol.

The cells also contains low-affinity Fe import pathways, the most important of which involves the plasma membrane proteins Fet4p.[6] Fet4p is induced by Aft1p in response to low concentrations of Fe in the growth medium.[7] The plasma-membrane protein Smf1p may constitute a second low-affinity Fe importer. This divalent metal transporter primarily transports Mn, but it can also transport Fe^{II}, albeit with low affinity.[8]

Most cytosolic Fe is sent to the mitochondria as these organelles are the primary site of ISC assembly and heme biosynthesis. Cytosolic Fe used for these processes is imported via the mitochondrial inner-membrane proteins Mrs3p/4p.[9] Many of the Fe-containing prosthetic groups that are generated in the mitochondria are installed into respiratory complexes.

Excess cytosolic Fe is transported into vacuoles. These organelles store and sequester Fe, then mobilize it as needed by the cell. The dominant form of Fe in the organelle is a mononuclear high-spin (HS) Fe^{III} complex with polyphosphate-related ligands.[10] Located on the vacuolar membrane, Ccc1p is the only known Fe importer of vacuolar Fe; however, Fe can also be imported to vacuoles via endocytosis.[11] Yap5p is an Fe-sensing protein that regulates the transcription of *CCC1* mRNA in response to cytosolic Fe.[12] *CCC1* mRNA is also regulated by Cth1p/2p; the binding of these proteins under Fe-limited conditions destabilizes the message, thereby preventing translation.[13]

Like all biological systems, yeast cells are commonly viewed as able to tightly regulate the import and trafficking of all cellular metabolites,[14] yet curiously such cells in glucose-containing media accumulate Fe continuously for two months.[15] To explore this unusual phenomenon, we used Mösbauer (MB) and EPR spectroscopies, as well as ICP-MS, to monitor the Fe content of yeast grown to various stages on rich (YPAD) and minimal media (MM). Exponentially growing cells maintained a constant level of cellular Fe due to a balance between cell growth and Fe import rates. In post-exponential growth phases, cell accumulated Fe, mainly as Fe^{III} oxyhydroxide nanoparticles and vacuolar HS Fe^{III} species. These effects were simulated semi-quantitatively by a mathematical model.

Experimental Procedures

Yeast Strain and Media

The primary strain used in this study was W303 (*MATα, ura3-1, ade2-1, trp1-1, his3-11,15, leu2-3,112*). Strain DY150 (FET3-GFP::KanMX[16]), isogenic to W303, was used to visualize Fet3-GFP. Cells were grown on standard YPAD with 2% (w/v) glucose and 40 mg/L adenine hemisulfate dihydrate agar plates for 3–4 days. For liquid cultures, YPAD and MM were prepared as described.[17] $^{56}Fe^{III}$- or $^{57}Fe^{III}$-citrate was added at 40 μM final

concentration. The endogenous Fe concentrations in YPAD and MM were 8 ± 3 μM and 0.20 ± 0.03 μM (n = 3), respectively.

Cell Growth and Mitochondria Isolation

Cell stocks were prepared in 15% glycerol and stored at −80 °C. As needed, frozen cells were scraped with a sterile wooded stick and spread onto an agar plate. Single colonies were used to inoculate 50 mL of YPD medium. Once grown, cultures were used to inoculate 1 L of YPAD or MM such that the initial OD_{600} ~ 0.01. In the experiment measuring the cellular Fe concentration during the first 14 hr of growth, 140 mL of YPD-grown cultures were used to inoculate 14 L of YPAD or MM in the fermenter. Medium glucose and cellular Fe concentrations were determined at over a 5 day period. Aliquots of cells were stored at −80 °C for Western blot analysis. For whole-cell Mösbauer studies, single colonies were directly inoculated into 1 L of medium and harvested at different times.

To isolate mitochondria, 1 L cultures were grown until OD_{600} ~ 1 at which point they were transferred into 24 L of MM at 30 °C in a stirred glass fermenter. The fermenter was purged with O_2 at 1 L/min. Cells were harvested after 5 days. Mitochondria were isolated in a refrigerated Ar-atmosphere glovebox as described.[17] Anaerobic solutions were degassed on a Schlenk line prior to being brought into the box. Isolated mitochondria were packed into Mössbauer cups[18] at 18,000×g for 30 min in an ultracentrifuge (Beckman Coulter Optima L-90K) with a swinging-bucket rotor (SW 32Ti, 32,000 RPM). Whole cells were similarly packed at 4,000×g for 5 min. The same spin conditions were used to pack cells into custom-made (4.2 mm OD, 3.0 mm ID, 80 mm long) suprasil quartz EPR tubes (Wilmad/Lab Glass, Buena, NJ, USA). Samples were frozen in liquid N_2 for later analysis.

Metal Content Analysis

Mitochondrial and whole-cell metal concentrations were measured by ICP-MS (Agilent Corp., 7700x). Packed mitochondria and whole cells were diluted 2-fold with water. 50, 75 and 100 μL of the resulting suspensions were incubated at 95 °C overnight in 200 μL of 30% trace-metal-grade HNO_3 and 100 μL of 35% trace-metal-grade HCl (both from Fisher Scientific). Samples were then diluted with 7.7 mL of distilled-deionized water. Resulting metal concentrations were adjusted for dilution relative to the packed material, and normalized using previously determined packing efficiencies of 0.70 for whole cells and 0.77 for mitochondria.[19] Reported concentrations should reflect those present in mitochondria and whole cells.

Glucose Assays

Glucose concentrations in growth medium were measured using the Autokit Glucose (439-90901, Wako Diagnostics) kit.[20] Culture medium was centrifuged at 16,000×g for 5 min to remove cells, and the supernatant was collected. 6.7 μL of cell-free medium was added to 1 mL of the kit assay mix. After incubating the reaction mixture at 37 °C for 5 min, the absorbance at 505 nm was measured, and that due to a water-blank was subtracted. Glucose concentrations in the growth medium were calculated using a standard curve, adjusting for dilution factors.

Western Blots

Fet3p expression levels were measured in membrane-protein extracts essentially as described.[21] Cell pellets were resuspended in an equivalent volume of extraction buffer (150 mM NaCl, 25 mM Tris-HCl (pH 7.4), 1% (v/v) protease inhibitor cocktail (P8340, Sigma) and 1 mM phenylmethanesulfonylfluoride) followed by an equal volume of 0.5 mm glass beads (Biospec Inc.; 0.5 mm diameter). The mixture was vortexed for 1 min then cooled on

ice for ≥ 1 min. This procedure was repeated 3 more times. Glass beads and unbroken cells were removed by centrifugation at 2,500×g for 5 min; then homogenates were spun at 16,000×g for 30 min at 4 °C. Pellets were resuspended in buffer containing 25 mM Tris-HCl (pH 7.4) and 1% Triton-X, and were kept at 4 °C overnight. Resultant solutions were centrifuged at 16,000×g and 4 °C for 30 min. Supernatants were collected as a clarified extract.

To determine Sod2p expression levels, whole-cell lysates were obtained as described above except that the glass beads and unbroken cells were removed by centrifugation for 10 min. Resulting supernatants were collected as a purified extract. Whole-cell lysates were assayed by the Oxyblot method as described below. Protein concentrations in extracts were measured using the BCA protein assay kit (Pierce). 60 μg of extract-proteins (16 μg for Sod2p assays) were resolved by 10% SDS-PAGE and transferred onto polyvinylidene fluoride membranes (Bio-Rad). Membranes were blocked with 1% casein and incubated with antibodies against Fet3p and Sod2p. Antibodies against Pma1p (Abcam, ab4645), actin (Abcam, ab8224), and Pgk1p (Invitrogen, 459250) were employed as loading controls. Developed membranes were imaged (FujiFilm LAS-4000 mini) and blot densities were quantified using ImageJ (National Institutes of Health) software. Unless noted otherwise, densities were normalized to the highest intensity band.

Oxyblot Assay

Whole-cell lysates were solubilized with 6% (w/v, final concentration) SDS and then mixed 1:1 with the 2,4-dinitrophenylhydrazine solution included in the Oxyblot assay kit (Millipore). DNP-derivatized proteins were resolved by SDS-PAGE followed by Western blot. Blot membranes were visualized using an antibody against DNP. The level of oxidative stress was quantified by densitometry.

Spectroscopy

Mösbauer spectra were recorded on MS4 WRC and LHe6T spectrometers (SEE Co., Edina, MN), the latter of which is capable of generating 0–6 T fields. Both were calibrated using α-Fe foil as described.[17] EPR spectra were recorded on an X-band EMX Plus spectrometer (Bruker Biospin, Billerica, MA). Spectra were re-scaled on SpinCount (ver. 3.0.13, http://www.chem.cmu.edu/groups/hendrich/facilities/index.html) using the ‘T-scale’ function which multiplies signal-intensity by temperature.

Results

We wanted to evaluate the Fe content of yeast cells grown in batch culture and harvested at different stages, including exponential and post-exponential growth modes. W303 cells grown on YPAD supplemented with 40 μM $^{57}Fe^{III}$ citrate grew exponentially with a doubling time (DT) of ~ 1.5 hr (Figure 1, circles). After *ca*. 11 hr, the growth rate started to decrease and cells transitioned to a slow-growing state with a DT of ~ 100 hr. The orange line in Figure 1 indicates the approximate time at which the transitionary period began; the purple line approximately demarcates the start of the slow-growth state. The glucose concentration in the culture (Figure 1B, triangles) declined exponentially during exponential growth such that the culture was virtually devoid of glucose during the slow-growth state. The observed diauxic growth pattern undoubtedly reflects a shift from fermentation to respiration.[22]

The concentration of Fe in the growing cell was also monitored, starting 4 doublings (~ 6 hr) after inoculation (Figure 1, squares). The Fe concentration during exponential growth was 300 – 400 μM (measured at OD = 0.1 – 1.0). In a follow-up experiment, the cellular Fe

concentration was also approximately invariant during exponential growth (Figure 1C), corresponding to the first 14 hrs of growth. For unknown reasons, the cellular Fe concentration for this batch of cells (~ 130 μM) was lower than in the first experiment, and the cells grew somewhat slower.

The cellular Fe concentration increased during the transitionary period (11 – 18 hr) at a rate of *ca*. 300 μM Fe/hr (slope of blue dashed line in Figure 1B), maximized at 2 – 2.5 mM, and then gradually decline at a rate of *ca*. −4 μM Fe/hr in the slow-growth state (Figure 1A, blue dashed line). With a DT of ~ 100 hr, this implies a constant slow-growth Fe import rate of ~ 20 μM Fe/hr.

We hypothesize that Fe accumulated during the transitionary period because of a mismatch of Fe import and cell growth rates. This implies that *the cell does not regulate these two rates perfectly*. They were well-regulated (i.e. synchronized) during exponential growth, such that the cellular Fe concentration remained constant. During the transitionary period, the Fe import rate declined slower than the cell growth rate declined, causing Fe to accumulate. Once in slow-growth mode, rates were again nearly matched, such that the Fe concentration of slow-growing cells was roughly invariant with time.

Our hypothesis accounts for these results *semi-quantitatively*. If exponentially growing cells contained 300 μM Fe and their DT was 1.5 hr, the Fe import rate should be 200 μM Fe/hr. If cells stopped growing while the Fe import rate remained unchanged, they should accumulate Fe at this rate (not at *ca*. 300 μM/hr as measured). If cells grew with a DT > 1.5 hr, they should still accumulate excess Fe but at a slower rate. These discrepancies arise because of significant batch-to-batch variations in growth rate and Fe concentration. Nevertheless, we favor this hypothesis because of its simplicity; alternatives would seem to require that Fe import rates increase during the transitionary period and then decrease during the subsequent slow-growth state. This scenario seems more complicated and less intuitive.

The Fet3p expression level, which reflects the activity of the high-affinity Fe import system, was also monitored. Expression was maximal during exponential growth but it declined gradually during the transitionary period and became undetectable during the slow-growth period (Figure 1B, diamonds and Figure S1A). These changes can also be explained by our hypothesis, namely that *Fe enters exponentially growing cells primarily through the high-affinity plasma-membrane Fe import system*. Since Fet3p is essentially not expressed during slow-growth mode, the slow-growth Fe import rate probably reflects one or more low-affinity Fe import system.

The same parameters were monitored for cells grown on MM. These cells grew more slowly during exponential phase (DT ≈ 2.0 hr) (Figure 2, circles). They transitioned at an OD_{600} ≈ 2 to a true stationary-state rather than to a slow-growth state. MM-grown cells consumed glucose more slowly, but the development of the transitionary period still correlated with a decline in glucose concentration (Figure 2B, triangles). The Fe concentration in exponentially growing MM cells (~ 400 μM measured at OD = 0.2) was similar to that observed for YPAD-grown cells while the rate of maximal Fe import during the transitionary period (100 μM/hr) was lower (slope of blue dashed line in Figure 2B). In a follow-up experiment, we observed that the Fe level was almost invariant during the initial 10 hrs of growth (Figure 2C).

Our hypothesis can again account for these results semi-quantitatively. A DT of 2 hr and an Fe concentration of 400 μM in exponentially growing cells imply an Fe import rate of 200 μM/hr, double the observed rate. Nevertheless, we continue to favor our hypothesis because alternatives are more complex and less intuitive.

The Fe concentration of MM-grown cells that just entered the stationary state was *ca*. 2 mM, similar to that of YPAD-grown cells. Unlike YPAD-grown cells, *MM-grown cells continued to accumulate Fe when in the stationary state*, such that they contained *ca*. 5 mM Fe after ~ 100 hr in this state. This corresponded to an average rate of ~ 30 μM Fe/hr. This stationary-state Fe import rate was similar to the slow-growth Fe import rate of YPAD-grown cells. Both probably originated from Fe entering via a low-affinity Fe import system which likely dominates during post-exponential growth modes.

Fet3p expression in MM-grown cells was maximal during exponential growth and declined rapidly thereafter (Figure 2B, diamonds, and Figure S1B). With 40 μM Fe in the medium, we find it remarkable that the high-affinity Fe import system was expressed at all; no Fet3p expression was previously observed in MM-grown cells harvested during late exponential or early transitionary phase (OD ~ 1.2).[23] When cells are grown in Fe-adequate medium, the high-affinity system might only be expressed during early exponential growth. Our hypothesis can explain the faster rate of FET3 shutdown along with the slower rate of growth shutdown and a similar concentration of Fe in YPAD- and MM-grown cells at the end of the transitionary period. Accordingly, shut-down of the high-affinity import system and the cell growth rate are probably better synchronized in MM-grown cells. As a loading control, we used Pma1p, an ATPase which is typically used as a plasma-membrane marker (Figure S1). However, its expression level varied with harvest time. We loaded the same amount of protein into each lane based on measured protein concentrations such that blot densities from one lane to another can be compared.

In contrast to Fe, neither Cu, Mn, nor Zn ions accumulated in 1-day-old or 5-day-old YPAD or MM cells. The concentration of Zn actually declined during the transition from exponential to stationary growth modes (Figure S2). This decline was gradual in YPAD cells, and was preceded by a spike in concentration (Figure S2, squares). In MM cells, there was no spike and the decline was more dramatic (Figure S2, circles). We have not established the molecular basis for these effects. However, if yeast cells contain a Zn efflux pump (e.g. homologous to ZnT1, a mammalian Zn efflux protein[24]), it may activate during post-exponential growth. Alternatively, Zn influx pathways may shut-down as cell growth slows.

We next used Mössbauer (MB) spectroscopy to evaluate the form(s) of Fe that accumulated in yeast grown to high culture densities on YPAD and MM. The 5 K low-field MB spectrum of YPAD-grown cells harvested in early transitionary phase (OD = 2.1) (Figure 3A) was dominated (79% of spectral intensity) by a sextet assigned to the mononuclear HS Fe^{III} species located in vacuoles.[10] The brown line above the spectrum simulates this feature.

The spectrum also exhibited a quadrupole doublet from nonheme high-spin (NHHS) Fe^{II} ions (8%, purple line) and the so-called *central doublet* or CD (9%, green line). The latter feature arises from S = 0 $[Fe_4S_4]^{2+}$ clusters plus low spin (LS) heme Fe^{II} ions (the two types of species cannot be distinguished).[25] A minor contribution from HS Fe^{II} hemes (3%, yellow line) could also be discerned. The CD and heme components are due primarily to mitochondrial respiratory complexes. The location of the NHHS Fe^{II} species has not been established. Fitting parameters and associated cellular Fe concentrations are given in Table S1.

The MB spectrum exhibited by YPAD-grown cells harvested in the late transitionary period (at OD = 3.2) exhibited the same general features (Figure 3B), as well as a new quadrupole doublet (19%, blue line) with parameters ($\delta \approx 0.53$ mm/s, $\Delta E_Q \approx 0.50$ mm/s) typical of Fe^{III} phosphate/polyphosphate-associated oxyhydroxide nanoparticles. The Fe concentration of these cells was higher than those harvested at OD = 2.1 (1.0 *vs*. 0.7 mM). The bulk of the

additional Fe was present as nanoparticles, as evidenced by the difference spectrum of Figure 3C.

YPAD-grown cells harvested 3 days later in the slow-growth state (OD = 8.0) exhibited a similar MB spectrum (Figure 3D) but with ~ 50% higher percent-effect, consistent with the higher concentration of Fe in the sample (1.5 mM). The difference spectrum (Figure 3E, slow-growth minus transitionary) revealed that the Fe that accumulated during this period was mainly in the form of the CD and mononuclear HS Fe^{III}. The absolute concentration of CD-associated Fe in YPAD-grown slow-growth cells was twice that in transitionary cells (Table S1). The generation of more mitochondrial Fe for cells in the slow-growth phase is consistent with the greater use of respiratory complexes after the diauxic shift.

The MB spectrum of MM-grown cells harvested in exponential phase (OD = 0.2) exhibited a similar distribution of Fe as in YPAD-grown cells, except that the percentage of Fe due to the CD was slightly higher (15% of spectral intensity) (Figure 4A). MM-grown cells harvested at later stages of exponential growth (Figure 4B, OD = 1.2) exhibited virtually the same spectrum. This is evidence that *the distribution of Fe in the cell is constant during exponential growth phase*. A similar distribution has been reported for cells harvested towards the end of exponential growth (at OD ~ 1.0).[23,26]

The Fe distribution of MM-grown cells changed as the cells moved into the transitionary phase (Figure 4C). Overall spectral intensity increased due to the higher Fe concentrations in these cells. The difference spectrum (Figure 4D, transitionary minus exponential) revealed that Fe^{III} nanoparticles and NHHS Fe^{II} ions (and some mononuclear HS Fe^{III} ions) mainly accumulated. This caused the percentage of Fe due to the CD in these spectra to decline; however, the absolute concentration of the CD increased somewhat.

The MB spectrum of 5-day MM-grown cells in stationary phase (Figure 4E) was intense, consistent with the tremendous buildup of Fe evident in Figure 2 at 120 hr. The primary form of Fe that accumulated was mononuclear HS Fe^{III} originating from vacuoles. The absolute concentration of Fe^{III} nanoparticles also increased, but there was no percentagewise increase.

After removing the contributions from these two dominating components (and the CD), the residuals revealed some broad unresolved absorption corresponding to the difference between the black hashmarks and the red line in Figure 4E. We collected a 100 K spectrum in hopes that this feature would collapse into a doublet, as is observed for ferritin[27], but it did not (Figure S3). This suggests a somewhat higher blocking temperature for the associated particles. We collected the low-temperature high-field (6 T) MB spectrum of an equivalent sample (Figure 4F) to overcome any spin-spin interaction due to high Fe concentration and to better characterize this elusive species. However, the spectrum was dominated (72% of overall intensity) by the HS Fe^{III} sextet, such that the less intense, broad unresolved feature could not be characterized.

The EPR spectrum of an equivalent sample (5-day old MM-grown WT cells harvested at stationary state) provided additional characterization of the broad unresolved species. The spectrum exhibited a derivative-like feature at g ~ 2.0 along with an intense signal at g = 4.3 (Figure 5A). The latter signal arose from the HS Fe^{III} species whose sextet dominated the MB spectrum of Figure 4E. The g ~ 2 signal probably arose from the same species that exhibited the broad unresolved MB feature. The EPR signal was reminiscent of that originating from Fe^{III} phosphate/polyphosphate-associated oxyhydroxide nanoparticles present in mitochondria of various ISC mutants.[17,28] However, the lineshape and temperature-dependence were somewhat different. Like the EPR signal of ISC mutant

nanoparticles, the new signal exhibited inverse Curie Law behavior. The effect was less dramatic relative to the ISC mutant signal, but the Curie Law behavior of the g = 4.3 signal allowed us to use it as an internal standard. Although much remains to be learned regarding the broad unresolved MB specie that gives rise to the g ~ 2 EPR signal, we suggest that it arises from a somewhat different form of Fe^{III} nanoparticles relative to that present in ISC-mutant mitochondria.[17,28,29]

The MB spectrum of cells grown on MM that contained 400 μM ^{57}Fe (10 times normal) was more intense than the corresponding spectrum of cells grown with 40 μM ^{57}Fe in the medium; the spectral lineshape was also different (Figure 6A). The MM sample grown on 400 μM ^{57}Fe contained ~ 28 mM Fe, *ca*. 3.5 times higher than the Fe concentration of cells grown on MM that contained 40 μM ^{57}Fe. About half of the spectral intensity was due to a broad doublet in the center of the spectrum, indicating ICS-mutant-type nanoparticles. About 9% of spectral intensity was due to mononuclear HS Fe^{III} species. Subtracting these two features from the spectrum revealed a broad unresolved magnetic feature between −5 and +7 mm/s representing ~ 30% of the original spectral intensity (Figure 6B). This feature was similar to the less intense broad unresolved feature in Figure 4E that could not be characterized well. The 6 T MB spectrum (Figure 6C) was again broad and poorly resolved. Approximately 90% of the spectral intensity arose from Fe^{III} nanoparticles, with the remaining intensity due primarily to mononuclear HS Fe^{III}. The HS-Fe^{III}-subtracted difference spectrum (Figure 6D, hashmarks) revealed broad absorption, albeit distinct from the 6 T MB spectrum of mitochondrial nanoparticles (Figure 6D, dotted line). We are unable to decompose the spectrum further, but conclude that the sample grown on MM supplemented with 400 μM ^{57}Fe contained more than one type of Fe^{III} oxyhydroxide nanoparticles. The X-band EPR spectrum of an equivalent sample (Figure 5B) exhibited an intense broad signal at g ~ 2 that again displayed inverse Curie Law behavior. The lineshape and temperature dependence of this signal differed from that present in spectra of nanoparticles found in ISC-mutant mitochondria, again indicating different magnetic properties and thus different structure/composition. The signal is similar to that exhibited by 5-day old MM cells grown on 40 μM ^{57}Fe.

Mitochondria were isolated from 5-day-old MM-grown cells in stationary state to determine whether they contained nanoparticles. The yield was low because the cell walls were thick and difficult to break. The sample exhibited the MB spectrum shown in Figure S4. The overall percent effect was very low, with about 40% of spectral intensity due to nanoparticles and about 45% due to the CD and possibly with a small contribution from $[Fe_2S_2]^{2+}$ clusters.[23] Although a substantial percentage of the Fe in these mitochondria was present as nanoparticles, this was far less (percentagewise and in absolute concentration) than the amount of nanoparticles that accumulate in ICS mutant mitochondria.[17,28,29] Thus, nanoparticles do not accumulate in stationary-state WT mitochondria to anywhere near to the extent that they do in mitochondria from ISC mutant strains. We conclude that the majority of nanoparticles present in 5-day-old MM-grown whole WT cells harvested in stationary state are not located in mitochondria.

Oxidative Stress in Post-Exponential Cells

Cells grown on YPAD for 5 days exhibited a similar level of oxidative damage compared with cells grown on the same medium for 1 day (Figure 7A, lane 2 vs. 1). This was unexpected given the higher Fe concentration in the 5-day-old cells. Cells grown on MM for 5 days actually experienced *less* oxidative damage than comparable 1 day old cells (Figure 7A, lane 4 vs. 3). This was also unexpected because MM-grown cells in stationary state contained much higher Fe concentrations than did MM-grown cells harvested in exponential and transitionary phases.

As loading controls, we tried 3-phosphoglycerate kinase (PGK1) and actin for whole cell extracts, and porin for mitochondrial extracts (Figure 7 and S5). However, none was ideal, because their expression levels varied with harvest time. PGK1 varied less than the others and so we show it in Figure 7. As with the oxyblot band of lane 4, the loading control also showed a decline at 5 days relative to 1 day, raising the question whether 5-day-old cells had less oxidative damage than 1-day-old cells, or about the same level. A second experiment (Figure 7B) indicated a decrease in the level of oxidative damage as MM-grown cells aged during the stationary period, and in this experiment the loading control was better behaved (Figure 7C). Thus, it appears that 5-day-old MM-grown cells suffer *less* ROS damage than 1-day old cells, a result that differed from our expectations. Also unexpected was the more general conclusion of this study, namely that *cellular Fe concentration is NOT an accurate predictor of ROS damage*. Metabolic activity, the growth medium and duration of growth may also be important factors.

We wondered whether the higher ROS level in slow-growing YPAD cells, relative to in stationary-state MM cells, resulted because the YPAD cells were respiring (and thus generating more ROS), whereas 5-day old MM cells were less metabolically active. Might MM-grown cells be unable to undergo the diauxic shift and respire due to a lack of essential nutrients present in YPAD but absent in MM? Cellular Sod2p levels are up-regulated during the diauxic shift.[30] To examine whether MM cells also underwent this shift, we quantified the level of Sod2p in YPAD *vs*. MM cells. During 5 days of growth, Sod2p band intensities in both YPAD and MM cells gradually increased (Figure 7C). The Sod2p level in slow-growing YPAD cells was increased 10-fold relative to the same cells during exponential growth (Figure 7C, YPAD, 120 *vs*. 9 hr). The Sod2p level in MM cells also increased, in this case by 7.5-fold, between exponential and stationary phases (Figure 7C, MM, 120 *vs*. 9 hr). We conclude that like YPAD cells, MM cells also shift their metabolism from fermentation to respiration when glucose is depleted. This is supported by the slightly increased level of oxidative stress in mitochondria isolated from 5- vs. 1-day-old MM cells (Figure 7A, lane 6 vs. 5). However, we still don't have a good explanation for why 5-day old MM cells suffered less ROS damage than 1-day-old MM cells; perhaps metabolic activity declined while ROS-damage repair processes remained highly active.

Model Development

We have developed a chemically-based mathematical model to help interpret our results. In it, cellular Fe (Fe_{cell}) was divided into 4 components, including cytosolic (Fe_C), vacuolar (Fe_V), mitochondrial (Fe_M) iron, and nanoparticles (Fe_P); thus, $[Fe_{cell}] = [Fe_V] + [Fe_M] + [Fe_C] + [Fe_P]$. We wanted to simulate concentrations of each component and compare them to the concentration data obtained from our MB, EPR and ICP-MS studies. To do this, we first assigned each component of the model to an observed species. Fe_V was assigned to the vacuolar HS Fe^{III} species, Fe_M was assigned to the sum of the central doublet Fe and heme Fe (most of which is associated with mitochondria), and Fe_C was assigned to the observed NHHS Fe^{II} species. Fe_P was assigned to the sum of both types of nanoparticles that were observed. Two versions of the model were developed so that two possible locations of nanoparticles could be considered. In version *C*, nanoparticles were presumed to be generated in the cytosol from Fe_C whereas in version *V*, they were assumed to be generated in vacuoles from Fe_V. In both versions, the rate of nanoparticle formation was proportional to either $[Fe_C]$ or $[Fe_V]$ raised to the power *px*.

The chemical model (Figure 8) assumed two Fe import pathways called *HI* (high affinity) and *LO* (low affinity), with corresponding import fluxes R_{HI} and R_{LO}. Imported Fe, assumed to be Fe_C, was trafficked to mitochondria and vacuoles at independent rates. The simulated $[Fe_C]$ concentration resulted from a balance between the rates of Fe import, the rates of Fe

export into these two organelles, and the cell growth rate α. For version *C*, these chemical processes were included in the ordinary differential equations (ODEs)

$$\frac{d[Fe_C]}{dt} = R_{HI}\left(\frac{1}{1+\left(\frac{Fe_C}{K_C}\right)^{cs}}\right) + R_{LO} - k_M\left(\frac{1}{1+\left(\frac{[Fe_M]}{K_M}\right)^{ms}}\right)[Fe_C] - k_P[Fe_C]^{px} - (k_V+\alpha)[Fe_C]$$

$$\frac{d[Fe_V]}{dt} = k_V[Fe_C] - \alpha[Fe_V]$$

$$\frac{d[Fe_M]}{dt} = k_M\left(\frac{1}{1+\left(\frac{[Fe_M]}{K_M}\right)^{ms}}\right)[Fe_C] - \alpha[Fe_M]$$

$$\frac{d[Fe_P]}{dt} = k_P[Fe_C]^{px} - \alpha[Fe_P]$$

which describe the changes in concentrations of each Fe component in the model. A similar set of ODE's was constructed for version *V* (Figure S6), with similar results.

The rate of Fe import via *LO* was considered to be constant under all growth conditions whereas *HI* was homeostatically regulated by the function

$$\mathrm{Reg}_{-}(Fe_C, K_C, cs) = \frac{1}{1+\left(\frac{[Fe_C]}{K_C}\right)^{cs}}.$$

Reg– functions can be used as *surrogates* for regulatory processes for which the molecular details are not known or are overly complicated.[31] These functions allow regulation to be described by just 3 parameters, including the sensed form of Fe, the threshold concentration, and the sensitivity of the regulatory effect. In our model, two Reg– functions were employed, one that regulated the rate of Fe import into the cell and another that regulated the rate of Fe import into mitochondria. For the first, we assumed that Fe_C was the sensed form of Fe, K_C was the threshold concentration, and *cs* was the sensitivity. Due to this function, the Fe import rate through *HI* declines when $[Fe_C] > K_C$ and increases when $[Fe_C] < K_C$. For the second Reg– function, we assumed that Fe_M was the sensed form of Fe that regulates mitochondrial import, with threshold K_M and sensitivity factor *ms*.

Both *C* and *V* sets of ODEs were solved numerically using Maple 17 (Maplesoft Inc) software, but this could only be done after values for all 11 associated parameters (R_{HI}, R_{LO}, k_M, k_V, k_P, K_C, *cs*, K_M, *ms*, *px*, *α*) were assigned. Finding best-fit values involved an iterative fitting procedure. The data in Table 1 was the composite of results rather than raw data from any particular sample. An error function was developed for quantitative comparisons between the 24 data points of Table 1 (6 conditions × 4 Fe component concentrations) and the corresponding simulated concentrations. Parameter values were first guesstimated and then adjusted systematically to minimize this function. Parameters were divided into those that were common for both versions and all conditions of the model (R_{HI}, R_{LO}, K_C, *cs*, K_M, *ms*) and those that differed for different versions (k_P, *px*) and conditions (k_M, k_V, *α*). Best-fit parameter values and simulated concentrations are given in Table 1.

The Fe speciation in YAPD and MM cells growing under exponential growth and slow-growth/stationary state conditions were simulated (Figure 9). The first 5 hr of the simulation reflect exponential growth, while the next 115 hr reflect slow-growth for YAPD cells (Figure 9, A and B) and the stationary state condition for MM cells (Figure 9, C and D). These plots should be semi-quantitatively compared to those in Figures 1 and 2,

respectively. Simulated changes in Fe concentrations probably occurred more slowly than in real cells because the simulated Fe import and cell growth rates were adjusted simultaneously at 5 hr. In real cells, the growth rate declines quickly while the Fe import rate declines more slowly. The black dashed line in Figure 9B illustrates this effect in the extreme. Here, the growth rate was adjusted to zero at 5 hr while the Fe import rate was maintained at exponential growth conditions; the resulting increase in cellular Fe concentration was dramatic - more rapid Fe accumulation than observed in real cells.

Discussion

Lack of regulation of Iron in post-exponential cells

Our results and analysis demonstrate that Fe import in yeast is effectively unregulated when cells grown in batch culture transition to post-exponential growth states. They accumulated excess Fe during the transition to either a slow-growth post-diauxic state (for growth on YPAD medium) or to a true stationary state (for growth on MM medium). MM-grown cells continued to accumulate Fe when in stationary state. YPAD-grown cells probably also imported excess Fe in the slow-growth state, but this effect was counterbalanced by a non-zero growth rate. This evidence of unregulated Fe import is surprising, given the abundant evidence and commonly held assumption that all metabolites and components of a cell are tightly regulated under all growth conditions. This study shows that *iron is an exception to this rule*.

Several molecular-level phenomena may collectively give rise to this exceptional behavior. The low-affinity Fe import pathway dominates in post-exponential cells and the pathway does not appear to depend strongly on the growth rate of the cell. Thus, even as cells slow or stop growing, they continue to import Fe through this pathway.

This is certainly one means by which the cell does not regulate the import of Fe. However, the rate of Fe import by the low-affinity pathway is probably too slow to be primarily responsible for the strong accumulation of Fe observed during the transitionary period; the high-affinity pathway must also be (somehow) misregulated. The high-affinity Fe import pathway is operational and tightly regulated during exponential growth, as evidenced by the strong Fet3p expression and invariant cellular Fe concentration. We hypothesize that *the high-affinity pathway shuts-down during post-exponential growth more slowly than the cell's growth rate declines.* As a result of this mismatch, the cell accumulates Fe.

But why didn't the high-affinity import pathway shut-down in post-exponential growth conditions as cell growth declined? What went wrong? According to our results and simulations, this happened because the concentration of cytosolic Fe in exponentially growing cells did not increase as cells transitioned to slow- or stationary-states. Had this happened, the *Reg*$_-$ "valve" would have shut-down Fe import.

But why didn't the [Fe_C] concentration increase as cell growth slowed and Fe started to accumulate? We hypothesize that this was because much of the extra imported cytosolic Fe was converted (directly or indirectly) into nanoparticles. The cell cannot sense these aggregated precipitates and thus it cannot regulate their formation. (In fact, the extent of nanoparticle formation is "contra-regulated" – meaning that as the rate of Fe import declined in post-exponentially grown cells in response to cellular regulation, the rate of nanoparticle formation actually *increased*.) Nanoparticles are a "sink" for Fe; they remove Fe_C from the cytosol, creating a deficiency of this sensed form of cellular Fe. Thus, even as the effect of dilution declined (due to a decrease in cell growth), [Fe_C] did not increase and Reg$_-$ did not shutdown. The situation was different for cells growing exponentially. Here Fe import and trafficking were well regulated and controlled because few nanoparticles formed. Fe uptake

and cell growth rates were matched such that cellular Fe concentration was essentially invariant.

Our simulations provided quantitative support for this effect. In both early and late stages of exponential growth, the rates of Fe import into YPAD cells were unchanged. This was certainly true for R_{LO} but also for R_{HI}. The Fe import rate through *HI* is given by the product of R_{HI} and Reg_{-}. In our simulations, R_{HI} was fixed for all conditions at 330 μM/hr while Reg_{-} was unrestricted. In our optimized fits, Reg_{-} was *ca*. 50% open under both conditions ($[Fe_C]$ in the first and second rows of Table 1 was about 30 μM which equals K_C). Likewise, the rates of Fe import into the mitochondria and vacuoles remained unchanged (k_m and k_v were the same in the first and second rows). In contrast, the cell growth rate (given by α in Table 1) in late exponential stage of YPAD cells was about half of what it was in early exponential growth.

Fe import rates were better synchronized to cell growth as cells moved from late exponential phase to slow-growth stage. Specifically, the growth rate and the rates of Fe import into the cell all declined 10 fold, as did the rates of Fe import into vacuoles and mitos (compare simulation data in second and third rows of Table 1).

Connection to known regulatory systems

Our results show that the high-affinity Fe uptake system (as monitored by Fet3p expression) was functioning during exponential growth, even with an Fe^{III} citrate concentration of 40 μM in the medium. A previous study found that Fet3p was not expressed in cells grown on the same medium and harvested early in the transitionary period.[23] This is slightly different from what our model predicts (namely that the high-affinity system should still be active at this stage), but it would be consistent with our model if the cells used for the Fet3p Western blot had actually been harvested slightly later, in stationary-state.

The low-affinity system may involve Fet4p, a divalent metal transporter on the plasma membrane, and/or Smf1. Since Fet4p is still active when cells are grown with 1 mM Fe-containing media,[32] Fet4p appears to be responsible for Fe uptake in cells grown on high [Fe] media; under these conditions, cells express almost no Fet3p.[23] The variation of Fet4p expression with changes in growth mode needs to be evaluated, but we suspect that Fet4p is the major Fe importer during post-exponential growth.

High Blocking Temperature nanoparticles

We report here a second type of nanoparticle in WT cells grown to post-exponential conditions. These nanoparticles differ in terms of magnetic and probably structural/compositional properties relative to those formed in the mitochondria of ISC mutant strains. Although we don't understand these differences well, our results suggest a difference in blocking temperature (T_B).[27] ISC-mutant associated nanoparticles exhibit a quadrupole doublet at 5 K, suggesting $T_B < 5$ K whereas the second type of nanoparticle appears to be magnetic at 5 K, suggesting $T_B > 5$ K. Beyond that, the broad and unresolved MB and EPR signatures associated with the "high blocking temperature" (HBT) nanoparticles make further characterization difficult. Nor do we know their location in WT cells. A small proportion nanoparticles appears to be present in mitochondria (as evidenced in MB spectra of isolated WT mitochondria), but the amount was low relative to the overall concentration of nanoparticles present in these cells. The quantity present was far less than that which accumulates in mitochondria in ISC mutant strains. The majority of nanoparticles that formed in post-exponentially grown WT cells were non-mitochondrial.

Two locations for HBT nanoparticles seem likely, namely vacuoles and the cytosol, but at this point we cannot distinguish between them. Nishida *et al*. identified nanoparticles in vacuoles[33] and we have found that the Fe in vacuoles is indeed susceptible to nanoparticles formation (of the low blocking temperature type).[10] The source of this susceptibility is uncertain, but Fe^{III} polyphosphate (which is closely related to vacuolar Fe) forms nanoparticles at high pH (e.g. 7). The vacuolar lumen is acidic, with values between 4.5 and 5.5 typical.

A recent report indicates that aging and mitochondrial dysfunction are associated with an increase of vacuolar pH.[34] Post-exponential cells are old, raising the intriguing possibility that decreased acidity in vacuoles causes mononuclear HS Fe^{III} species in vacuoles to precipitate as nanoparticles. Losing a proton from a coordinated water could help generate a bridge between two mononuclear complexes. This process, occurring repeatedly throughout a population of HS Fe^{III} complexes, could cause nanoparticles to form. Since nanoparticles are precipitated aggregates, this process would be sensed by the cell as a *decline* of vacuolar Fe (despite the fact that Fe is accumulating), prompting additional Fe_C to be imported from the cytosol into the organelle.

Lack of correlation between iron accumulation and ROS damage

Iron is generally considered to be deleterious to the cell when in excess, because it can catalyze the formation of hydroxyl radicals and other ROS.[1] Indeed, we and others have linked ROS damage in mitochondria to nanoparticle formation in that organelle.[17,28,35] In our current study, we found no correlation between ROS formation and Fe accumulation. Vacuoles have an enormous capacity to store Fe; perhaps the sequestration of Fe into vacuoles prevents ROS from being generated. The same may not hold true for mitochondria. This organelle in WT cells appears to be more strictly regulated in terms of Fe, such that it does not normally accumulate massive quantities of nanoparticles. Nanoparticles generated in other non-mitochondrial compartments may not significantly damage the cell, suggesting that in a non-mitochondrial context, nanoparticles are more of a nuisance than a danger. Another consideration is that in slow-growing or stationary state cells, Fe-associated ROS may have been eliminated (by the ROS-response machinery of the cell) faster than it was generated.

Insights from the model

Although simple, the chemically-based mathematical model captured essential behavior of global Fe metabolism in *S. cerevisiae* cells. The model illustrated the balance of processes that determines the concentrations of the four major groups of Fe in the cell, namely cytosolic, mitochondrial, vacuolar, and nanoparticulate. These processes include high- and low-affinity import pathways, import into two organelles, conversion into nanoparticles, and the growth rate of the cell. The model predicted the distribution of the four major groups of Fe as observed by MB. The quantitative effects obtained by simulation can be rationalized qualitatively from the chemical model of Figure 8, viewing growth rate as an increase in cell volume that dilutes all cellular species.

Two versions of the model were considered, including one that assumed that nanoparticles form from cytosolic Fe_C (Version *C*) and one that assumed that they form from vacuolar Fe_V (Version *V*). Simulations using *C* fitted the data 22% better than those generated using version *V*, which suggests that nanoparticles form in the cytosol. However, we do not regard this as sufficient grounds to eliminate version *V*. There is no independent evidence that nanoparticles can form in the cytosol, whereas nanoparticles have been observed in isolated vacuoles.[10] Further studies are required to settle this issue.

R_{LO} contributed 30 μM/hr of Fe import under both exponential and post-exponential growth conditions. The low-affinity Fe import system was unregulated with respect to stages in cell growth. In contrast, the high affinity system R_{HI} was regulated (our model could not reproduce the data without including such regulation). The molecular-level details of this regulation are not well understood, so we employed a surrogate *Reg*₋ function to mimic the effect. Under YPAD and MM exponential conditions, R_{HI} imported Fe at a rate of ~ 150 μM/hr ($330 \cdot 1/(1+ (32/30)^3)$) corresponding to *ca*. 80% of total Fe influx. During slow-growth or stationary phases, simulations indicated that R_{HI} imported Fe at a rate of ~23 μM/hr ($310 \cdot 1/(1+ (70/30)^3)$), representing *ca*. 40% of total Fe influx.

The unusual situation that led to an unregulated condition occurred in the late-exponential/transitionary period. Here, $[Fe_C]$ was about the same as it was during exponential phase (i.e. the valve was *ca*. 50% open) even though cells were growing half as fast (and thus cellular component concentrations were being diluted half as fast). This caused the unregulated influx of Fe. $[Fe_C]$ did not increase, as would have otherwise occurred, because a substantial portion converted, either directly or indirectly, into nanoparticles. These particles are not sensed by the cell, yet they suppress the increase in $[Fe_C]$ that would otherwise shutdown Fe import. Thus, Fe continued to flow into the cell at the exponential-growth-mode level. This is the cause of unregulated Fe homeostasis in post-exponential yeast cells.

Previous studies and the importance of growth rate

In our previous studies, cells grown in medium containing ferric citrate concentrations as high as 10 mM did not show as high cellular Fe concentrations as we have observed here.[23] Why? In those studies, cells were harvested in late exponential phase (OD = 1.2), perhaps before the Fe accumulation phenomenon became severe. Our current study reveals that the mode of growth *near the time of harvesting* is critically important in dictating the extent of Fe accumulation.

This study illustrates the importance of growth rate in understanding Fe import, trafficking, and regulation. Unfortunately, the time-dependence of regulation has not been emphasized in previous studies of cellular Fe metabolism. In many published studies involving the Fe metabolism of yeast, the exact growth mode and growth rate at the time of harvesting are not even mentioned. We show here that such information will be important for accurately interpreting the phenotype of various Fe-associated mutant strains. The excess Fe that accumulates in yeast cells during post-exponential growth periods could confuse such interpretations and obscure the primary function of the mutated protein, a typical objective of such studies. In the future, those studying Fe metabolism in yeast should ideally focus on the Fe content of *exponentially* growing cells to provide insight into Fe-related metabolism and the primary function of associated proteins. During exponential growth, nanoparticle formation is minimal such that regulatory effects will not be distorted.

Is the lack of iron regulation in cells unique?

Virtually all cellular reactions are enzyme-catalyzed and thus are genetically (and/or allosterically) regulated by the cell. Importantly, enzyme-catalyzed reactions are generally orders-of-magnitude faster than non-catalyzed reactions. Because of this, non-catalyzed reactions are generally irrelevant from the cell's perspective; the cell is living in a faster time domain. Iron evades cellular control because nanoparticles can form *rapidly* via non-enzymatically catalyzed reactions, at rates that depend on very general chemical properties of the cell such as pH and redox status. The cell has no means of sensing this formation apart from the indirect (and distorting) effect that it has on cytosolic Fe concentrations. Thus, in the case of Fe, *the cell simply tolerates a bit of chaos*. Fortunately, such nanoparticle-forming reactions are not lethal as they do not generate toxic levels of ROS.

Although we cannot state unequivocally that this lack of cellular regulation is unique for Fe, we are unaware of other cellular metabolites that are unregulated. Such an occurrence for another cellular component would seem to require a similar combination of reaction chemistry which we regard as highly unlikely.

Supplementary Material

Refer to Web version on PubMed Central for supplementary material.

Acknowledgments

Funding Sources

This study was funded by the National Institutes of Health (GM084266), the National Science Foundation (DMS-0714896) and the Robert A. Welch Foundation (A1170).

We thank Andrew Dancis (University of Pennsylvania) for providing the DY150 strain and the Fet3p antibody, Valeria Culotta (Johns Hopkins University) for providing the Sod2p antibody, and Brad Pierce (University of Texas, Arlington) for allowing us to use his EPR spectrometer.

ABBREVIATIONS

CD	central doublet
DNP	2,4-dinitrophenyl
DT	doubling time
EPR	electron paramagnetic resonance
HI	high affinity pathway
HBT	high blocking temperature
HS	high spin
ICP-MS	inductively coupled plasma mass spectrometry
ISC	iron sulfur cluster
LO	low affinity pathway
LS	low spin
MB	Mösbauer
MM	minimal medium
NHHS	nonheme high spin
OD	optical density
ODE	ordinary differential equation
ROS	reactive oxygen species
YPAD	yeast extract, peptone, adenine hemisulfate, and dextrose
WT	wild type

References

1. Imlay JA. Pathways of oxidative damage. Annu Rev Microbiol. 2003; 57:395–418. [PubMed: 14527285]

2. Van Ho A, Ward DM, Kaplan J. Transition metal transport in yeast. Annu Rev Microbiol. 2002; 56:237–261. [PubMed: 12142483]
3. Lill R, Mühlenhoff U. Maturation of iron-sulfur proteins in eukaryotes: Mechanisms, connected processes, and diseases. Annu Rev Biochem. 2008; 77:669–700. [PubMed: 18366324]
4. Stearman R, Yuan DS, Yamaguchi-Iwai Y, Klausner RD, Dancis A. A permease-oxidase complex involved in high-affinity iron uptake in yeast. Science. 1996; 271:1552–1557. [PubMed: 8599111]
5. Shakoury-Elizeh M, Tiedeman J, Rashford J, Ferea T, Demeter J, Garcia E, Rolfes R, Brown PO, Botstein D, Philpott CC. Transcriptional remodeling in response to iron deprivation in *Saccharomyces cerevisiae*. Molecular Biology of the Cell. 2004; 15:1233–1243. [PubMed: 14668481]
6. Dix DR, Bridgham JT, Broderius MA, Byersdorfer CA, Eide DJ. The FET4 gene encodes the low-affinity Fe(II) transport protein of *Saccharomyces cerevisiae*. J Biol Chem. 1994; 269:26092–26099. [PubMed: 7929320]
7. Waters BM, Eide DJ. Combinatorial control of yeast FET4 gene expression by iron, zinc, and oxygen. J Biol Chem. 2002; 277:33749–33757. [PubMed: 12095998]
8. Cyert MS, Philpott CC. Regulation of cation balance in *Saccharomyces cerevisiae*. Genetics. 2013; 193:677–713. [PubMed: 23463800]
9. Froschauer EM, Schweyen RJ, Wiesenberger G. The yeast mitochondrial carrier proteins Mrs3p/Mrs4p mediate iron transport across the inner mitochondrial membrane. Biochimica et Biophysica Acta (BBA) - Biomembranes. 2009; 1788:1044–1050.
10. Cockrell AL, Holmes-Hampton GP, McCormick SP, Chakrabarti M, Lindahl PA. Mössbauer and EPR study of iron in vacuoles from fermenting *Saccharomyces cerevisiae*. Biochemistry. 2011; 50:10275–10283. [PubMed: 22047049]
11. Li LT, Chen OS, Ward DM, Kaplan J. CCC1 is a transporter that mediates vacuolar iron storage in yeast. J Biol Chem. 2001; 276:29515–29519. [PubMed: 11390404]
12. Li L, Bagley D, Ward DA, Kaplan J. Yap5 is an iron-responsive transcriptional activator that regulates vacuolar iron storage in yeast. Mol Cell Biol. 2008; 28:1326–1337. [PubMed: 18070921]
13. Puig S, Askeland E, Thiele DJ. Coordinated remodeling of cellular metabolism during iron deficiency through targeted mRNA degradation. Cell. 2005; 120:99–1df10. [PubMed: 15652485]
14. Kosman DJ. Molecular mechanisms of iron uptake in fungi. Mol Microbiol. 2003; 47:1185–1197. [PubMed: 12603727]
15. Reverter-Branchat G, Cabiscol E, Tamarit J, Ros J. Oxidative damage to specific proteins in replicative and chronological-aged *Saccharomyces cerevisiae* - Common targets and prevention by calorie restriction. J Biol Chem. 2004; 279:31983–31989. [PubMed: 15166233]
16. Felice MR, De Domenico I, Li LT, Ward DM, Bartok B, Musci G, Kaplan J. Post-transcriptional regulation of the yeast high affinity iron transport system. J Biol Chem. 2005; 280:22181–22190. [PubMed: 15817488]
17. Miao R, Kim H, Koppolu UMK, Ellis EA, Scott RA, Lindahl PA. Biophysical characterization of the iron in mitochondria from Atm1p-depleted *Saccharomyces cerevisiae*. Biochemistry. 2009; 48:9556–9568. [PubMed: 19761223]
18. Lindahl, PA.; Morales, JG.; Miao, R.; Holmes-Hampton, G. Isolation of Saccharomyces cerevisiae mitochondria for Mössbauer, EPR, and electronic absorption spectroscopic analyses. In: Allison, WS., editor. Methods in Enzymology, Vol 456: Mitochondrial Function, Part A: Mitochondrial Electron Transport Complexes and Reactive Oxygen Species. 2009. p. 267-285.
19. Miao R, Holmes-Hampton GP, Lindahl PA. Biophysical investigation of the iron in Aft1-1(up) and Gal-YAH1 *Saccharomyces cerevisiae*. Biochemistry. 2011; 50:2660–2671. [PubMed: 21361388]
20. Kitagaki H, Cowart LA, Matmati N, Montefusco D, Gandy J, de Avalos SV, Novgorodo SA, Zheng J, Obeid LM, Hannun YA. ISC1-dependent metabolic adaptation reveals an indispensable role for mitochondria in induction of nuclear genes during the diauxic shift in *Saccharomyces cerevisiae*. J Biol Chem. 2009; 284:10818–10830. [PubMed: 19179331]
21. Singh A, Severance S, Kaur N, Wiltsie W, Kosman DJ. Assembly, activation, and trafficking of the Fet3p•Ftr1p high affinity iron permease complex in *Saccharomyces cerevisiae*. J Biol Chem. 2006; 281:13355–13364. [PubMed: 16522632]

22. Yoon H, Klinzing G, Blanch HW. Competition for mixed substrates by microbial-populations. Biotechnol Bioeng. 1977; 19:1193–1210. [PubMed: 884234]
23. Holmes-Hampton GP, Jhurry ND, McCormick SP, Lindahl PA. Iron content of *Saccharomyces cerevisiae* cells grown under iron-deficient and iron-overload conditions. Biochemistry. 2013; 52:105–114. [PubMed: 23253189]
24. Palmiter RD, Huang LP. Efflux and compartmentalization of zinc by members of the SLC30 family of solute carriers. Pflugers Archiv-European Journal of Physiology. 2004; 447:744–751. [PubMed: 12748859]
25. Holmes-Hampton GP, Miao R, Morales JG, Guo YS, Münck E, Lindahl PA. A nonheme high-spin ferrous pool in mitochondria isolated from fermenting *Saccharomyces cerevisiae*. Biochemistry. 2010; 49:4227–4234. [PubMed: 20408527]
26. Park J, McCormick SP, Chakrabarti M, Lindahl PA. Insights into the iron-ome and manganese-ome of Δ*mtm1 Saccharomyces cerevisiae* mitochondria. Metallomics. 2013; 5:656–672. [PubMed: 23598994]
27. Papaefthymiou GC. The Mösbauer and magnetic properties of ferritin cores. Biochimica et Biophysica Acta (BBA) - General Subjects. 2010; 1800:886–897.
28. Miao R, Martinho M, Morales JG, Kim H, Ellis EA, Lill R, Hendrich MP, Münck E, Lindahl PA. EPR and Mössbauer spectroscopy of intact mitochondria isolated from Yah1p-depleted *Saccharomyces cerevisiae*. Biochemistry. 2008; 47:9888–9899. [PubMed: 18717590]
29. Lesuisse E, Santos R, Matzanke BF, Knight SAB, Camadro JM, Dancis A. Iron use for haeme synthesis is under control of the yeast frataxin homologue (Yfh1). Hum Mol Genet. 2003; 12:879–889. [PubMed: 12668611]
30. Flattery-O'Brien JA, Grant CM, Dawes IW. Stationary-phase regulation of the *Saccharomyces cerevisiae* SOD2 gene is dependent on additive effects of HAP2/3/4/5- and STRE-binding elements. Mol Microbiol. 1997; 23:303–312. [PubMed: 9044264]
31. Jhurry ND, Chakrabarti M, McCormick SP, Gohil VM, Lindahl PA. Mösbauer study and modeling of iron import and trafficking in human Jurkat cells. Biochemistry. 2013
32. Dix D, Bridgham J, Broderius M, Eide D. Characterization of the FET4 protein of yeast - Evidence for a direct role in the transport of iron. J Biol Chem. 1997; 272:11770–11777. [PubMed: 9115232]
33. Nishida K, Silver PA. Induction of biogenic magnetization and redox control by a component of the target of rapamycin complex 1 signaling pathway. PLoS Biol. 2012:10.
34. Hughes AL, Gottschling DE. An early age increase in vacuolar pH limits mitochondrial function and lifespan in yeast. Nature. 2012; 492:261–265. [PubMed: 23172144]
35. Bulteau AL, Dancis A, Gareil M, Montagne JJ, Camadro JM, Lesuisse E. Oxidative stress and protease dysfunction in the yeast model of Friedreich ataxia. Free Radic Biol Med. 2007; 42:1561–1570. [PubMed: 17448903]

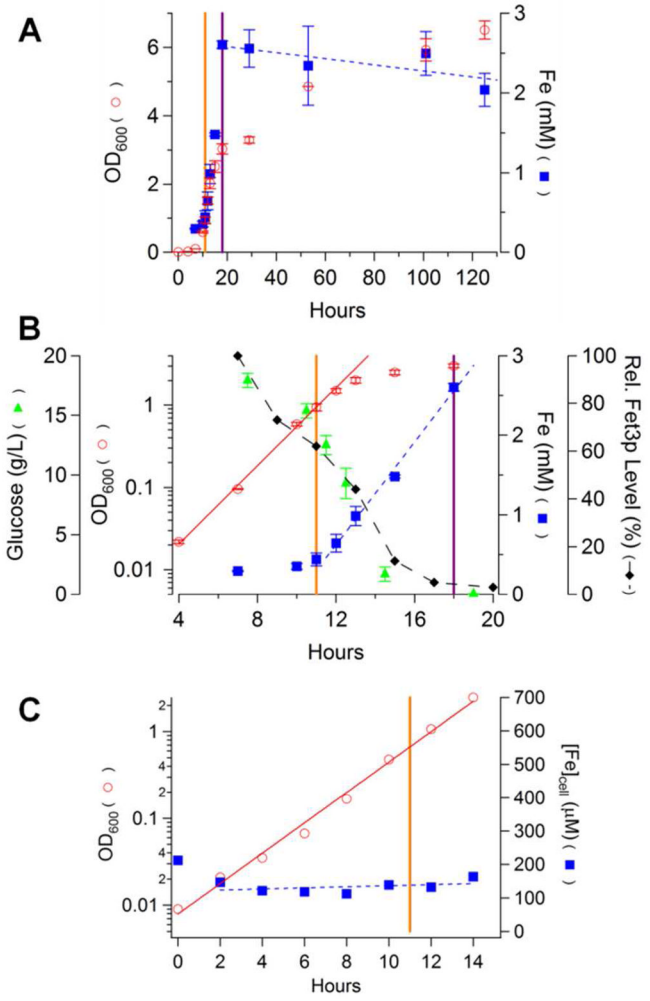

Figure 1.

Chronological profile of nutrient, growth and Fe-associated parameters for cells grown in batch culture on YPAD for 5 days. A, full plots; B, zoom of 4 – 20 hr; C, 0 – 14 hr for a follow-up experiment. Data include OD_{600} (circles), cellular Fe concentration (squares), glucose concentration (triangles) and Fet3p expression (diamonds). Orange vertical lines demarcate exponential and transitionary modes; purple lines demarcate transitionary and slow-growing modes. Plotted OD_{600} and iron(glucose) concentrations in A and B were the average of two(three) independent experiments. Bars indicate standard deviation.

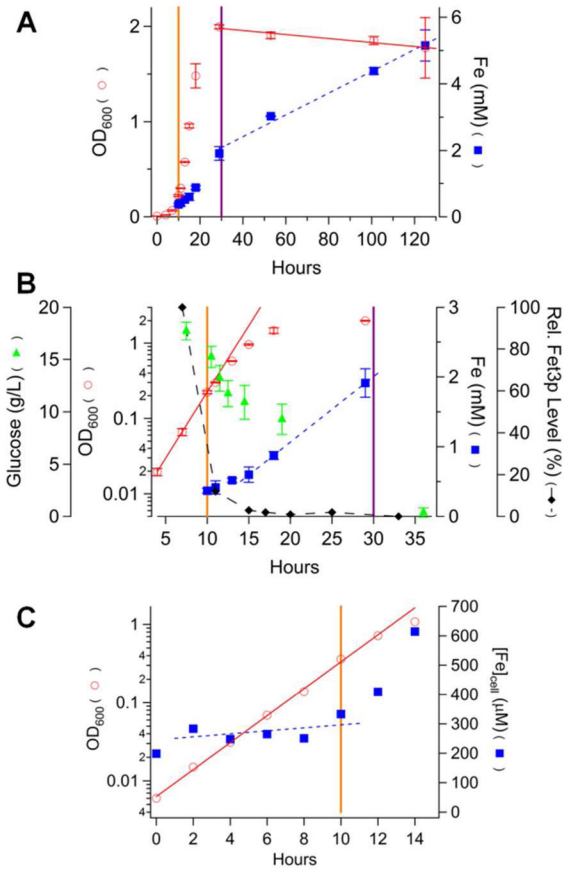

Figure 2.

Chronological profile of nutrient, growth and Fe-associated parameters for cells grown in batch culture on MM for 5 days. A, full plots; B, zoom of 5 – 35 hr; C, 0 – 14 hr for a follow-up experiment. Data symbols and lines are the same as in Figure 1. Reported OD_{600} and iron(glucose) concentrations in A and B were the average of two(three) independent experiments. Bars indicate standard deviation.

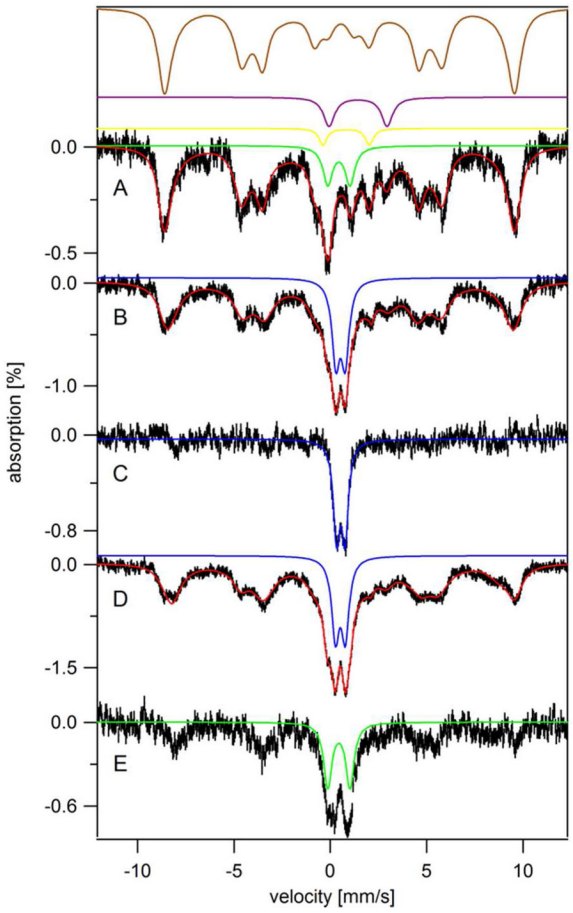

Figure 3.

5 K 0.04 T Mösbauer spectra of whole yeast cells grown on YPAD and harvested at various time points. A, early transitionary phase (OD 2.1); B, late transitionary phase (OD 3.2); C, B-minus-A difference spectrum; D, post-diauxic growth phase (OD 8.0); E, D-minus-B difference spectrum. Red lines simulate collectively the spectral features associated with HS Fe^{III}, NHHS Fe^{II}, HS Fe^{II} heme, CD, and Fe^{III} nanoparticles. Brown, purple, yellow, green and blue lines are simulations of HS Fe^{III}, NHHS Fe^{II}, HS Fe^{II} heme, the central doublet, and Fe^{III} nanoparticles, respectively. The field was applied parallel to γ-rays.

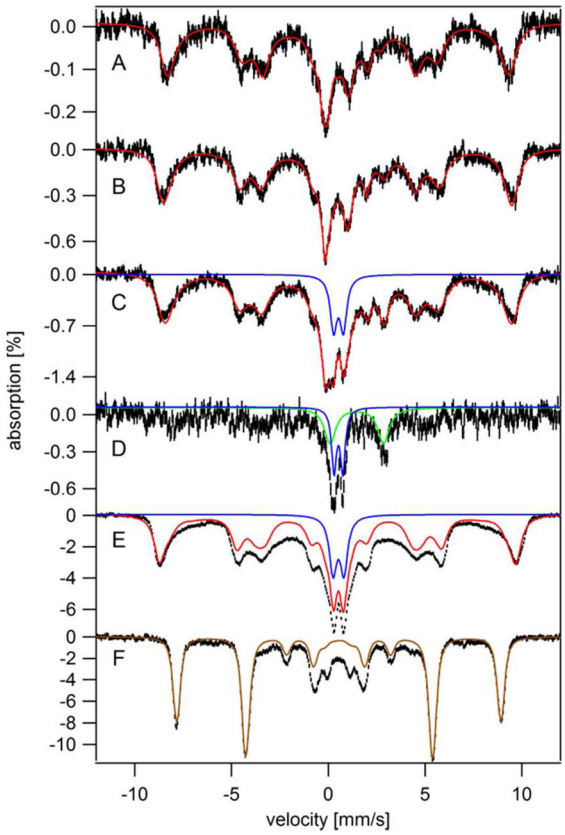

Figure 4.

Mössbauer spectra of whole yeast cells grown on MM and harvested at various time points. For A – E, the temperature was 5 K and a 40 mT field was applied parallel to γ-rays. For F, the temperature was 4.2 K and a 6 T field was applied perpendicular to the γ-rays. A, early exponential phase (OD 0.2); B, exponential phase (OD 1.2); C, transitionary phase (OD 1.8); D, C-minus-B difference spectrum (the spectral intensity of B was doubled and then subtracted from C) E, stationary phase (OD 1.8, 5-day-grown); F, an equivalent sample of E (OD 1.7, 5-day-grown). Red lines are composite simulations that include contributions from HS Fe^{III}, NHHS Fe^{II}, HS Fe^{II} heme, CD, and Fe^{III} nanoparticles. Blue and green lines simulate contributions from Fe^{III} nanoparticles and HS Fe^{II}, respectively. The brown line simulates the HS Fe^{III} species using $S = 5/2$, D = 0.15 cm^{-1}, E/D = 0.21, $A_0/g_N \cdot \beta_N = -233$ kG, $\delta = 0.55$ mm/s, $\Delta E_Q = 0.42$ mm/s, and $\eta = 1.3$.

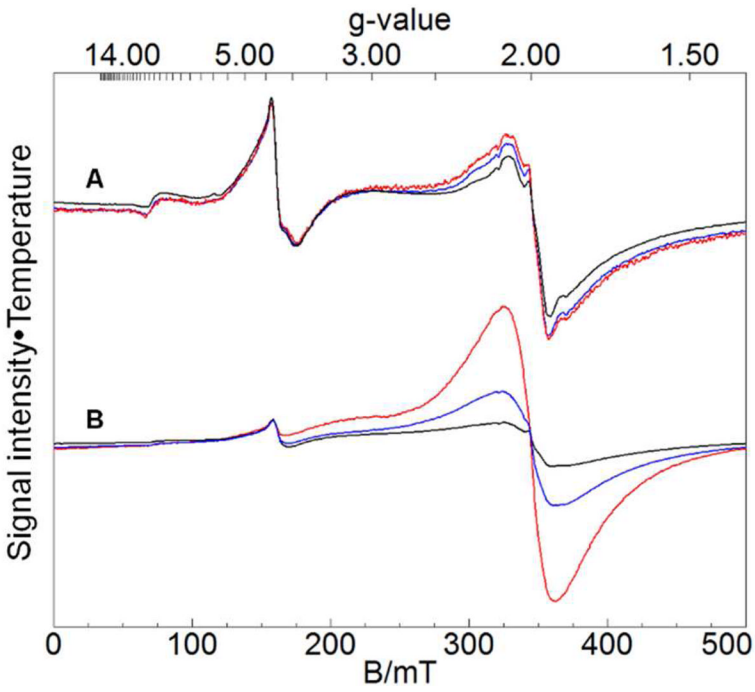

Figure 5.

X-band EPR spectra of 5-day-grown cells. A, grown on MM with 40 μM Fe; B, grown on MM with 400 μM Fe. Black, 10 K; blue, 30 K; red, 80 K. Spectra were recorded at 0.05 mW microwave power, 9.64 GHz frequency and 10 Gauss modulation amplitude, and then have been adjusted vertically so that the g = 4.3 resonances are aligned. Spectral intensities in A and B were multiplied by absolute temperature while those in A were additionally multiplied by 5 for presentation purposes.

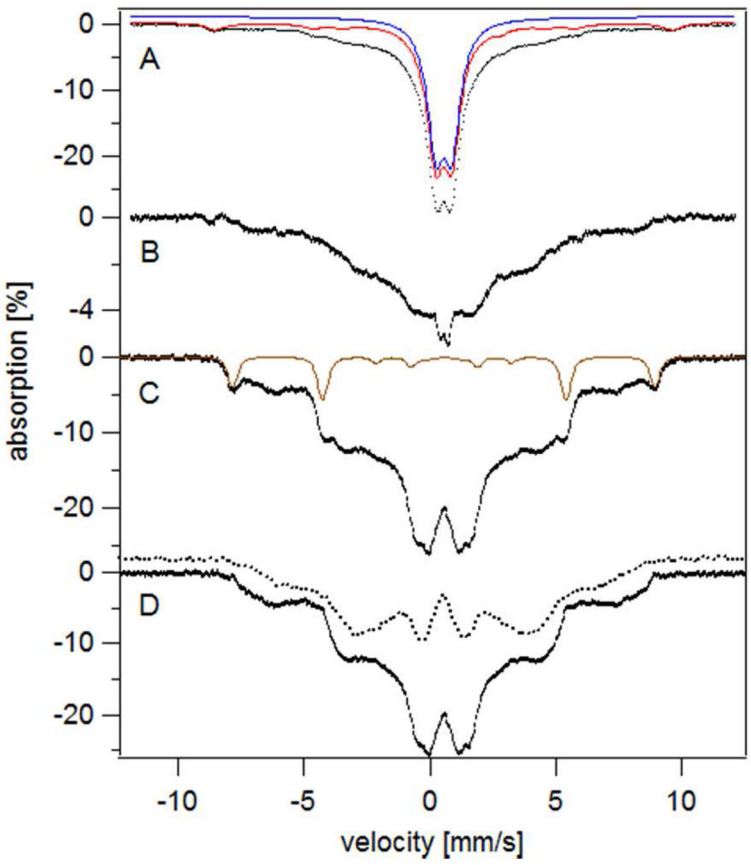

Figure 6.

Mösbauer spectra of MM-grown yeast cells at stationary phase. A, 400 μM Fe-containing MM-grown cells at stationary phase (OD 2.2, 5-day-grown). The red line simulates the contributions from HS Fe^{III}, Fe^{III} nanoparticles and the CD. The blue line simulates the ICS-mutant-type nanoparticles. B, same as A but after subtracting the red-line simulation. For A and B, the temperature was 5 K and a 40 mT field was applied parallel to γ-rays. C, same as A but at 6 T (transverse field) and 4.2 K; D, same as in C but the HS Fe^{III} component has been subtracted. Dotted line is the equivalent MB spectrum of isolated mitochondria from Aft1-1^{up} cells.[19] The brown line simulates the HS Fe^{III} contribution.

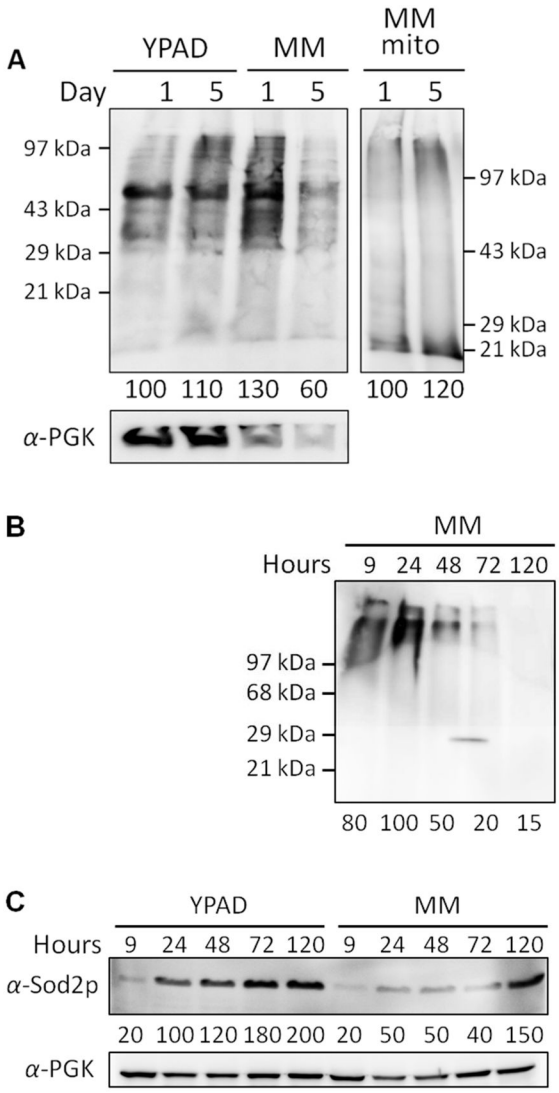

Figure 7.

Oxyblot and Western blot against Sod2p of whole cells and mitochondria harvested at different conditions. A, Oxyblot of whole-cell lysates (left panel) and mitochondrial extracts (right panel). Medium and days of growth are displayed on the top of blots. Overall band intensities (below blots) are indicated as percentages relative to YPAD/1 day (left) or MM/1 day (right) blots. B, Oxyblot time-course of whole cell lysates grown on MM. Band intensities (below blots) are indicated as percentages relative to that of MM/24 hr blot. The intensity at ~29 kDa between lanes 3–4 is an artifact. C, Western blot against Sod2p for YPAD and MM cells grown for different times (same MM samples as in B). Lane 1–5, YPAD; lane 6–10, MM; hours of growth are labeled on the top of each lane. Band intensities (below blots) are given as percentages relative to that of the YPAD/1 day blots. Each lane was developed with 4 (Oxyblot for whole cell lysates), 15 (Oxyblot for mitochondrial extracts) and 16 (Western blot against Sod2p for whole cell lysates) μg of protein.

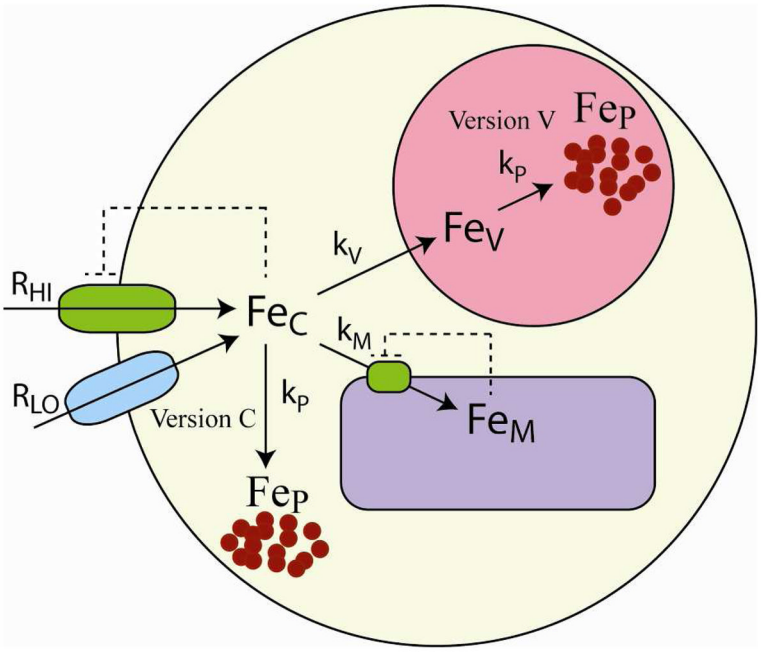

Figure 8.

Model of Fe trafficking in yeast cells. Fe from the medium enters via high-affinity (R_{HI}) and low-affinity (R_{LO}) pathways. R_{LO} is unregulated while R_{HI} is regulated by the concentration of cytosolic Fe (Fe_C), indicated by the dashed lines. Fe_C moves into the mitochondria and vacuoles, forming mitochondrial (Fe_M) and vacuolar (Fe_V) forms. The import of Fe_C into the mitochondria is regulated by the concentration of Fe_M. In version *C*, Fe^{III} nanoparticles (Fe_P) were assumed to form in cytosol whereas in version *V*, they were assumed to form in vacuoles. Rate-constants and other parameters are listed in Table 1.

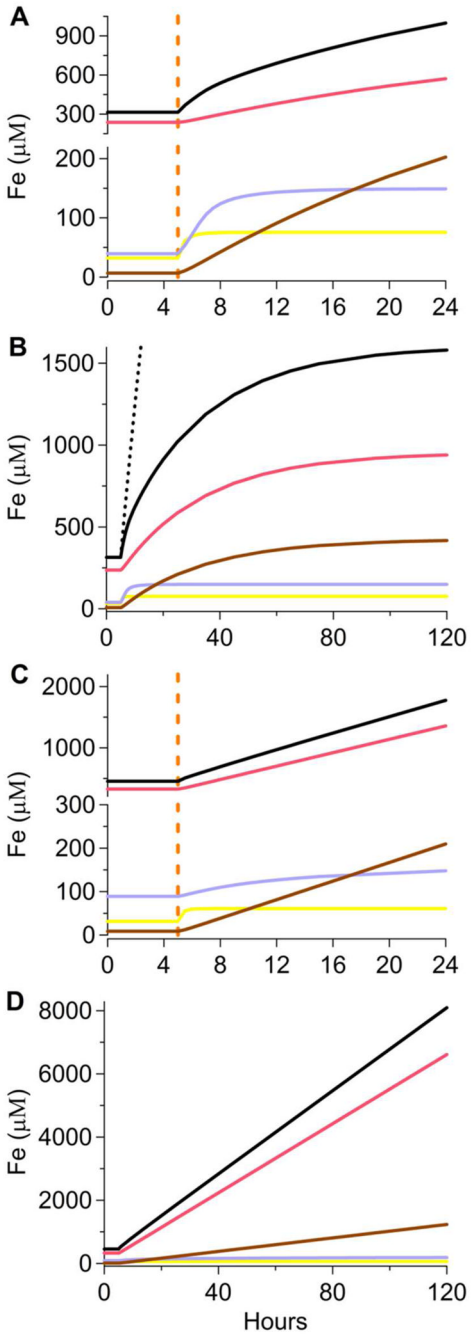

Figure 9.

Simulated kinetics of Fe uptake and trafficking in yeast cells. A, YPAD, 1-day-growth scale; B, YPAD, 5-day-growth scale; C, MM, 1-day-growth scale; D, MM, 5-day-growth scale. The first 5 hr (before the orange line) reflect exponential growth conditions while the remaining 115 hrs indicate slow-growth and steady-state modes. Black, pink, cyan, yellow, and brown lines indicate [Fe_{cell}], [Fe_V], [Fe_M], [Fe_C], and [Fe_P], respectively. Dashed line simulates [Fe_{cell}] when cell growth was set to zero while Fe import rates were set to those for exponential growth.

Table 1

Parameters for Simulations. Most of the composite data were obtained from the simulated percentages of MB spectra in Figures 3 and 4. Composite data of YPAD cells at early exponential growth mode were estimated by assuming that the Fe distribution in the cells was identical to that in the YPAD cells at late exponential growth mode.

	$[Fe_{cell}]$	$[Fe_C]$	$[Fe_M]$	$[Fe_P]$	$[Fe_V]$	k_v (hr^{-1})	k_M (hr^{-1})	α (hr^{-1})
YPAD, Early Exp.	300_D	24_D	40_D	0_D	236_D			
	314_C	32_C	40_C	5_C	234_C	4.8	0.8	0.65
	310_V	32_V	40_V	1_V	237_V			
YPAD, Late Exp	700_D	56_D	90_D	0_D	550_D			
	677_C	33_C	89_C	11_C	553_C	4.8	0.8	0.29
	667_V	33_V	84_V	7_V	543_V			
YPAD, Slow-growth	1500_D	75_D	150_D	285_D	990_D			
	1577_C	79_C	150_C	288_C	986_C	0.43	0.60	0.034
	1359_V	90_V	152_V	128_V	989_V			
MM, Exponential	430_D	13_D	90_D	0_D	327_D			
	454_C	31_C	89_C	6_C	327_C	5.2	1.6	0.50
	450_V	32_V	89_V	2_V	327_V			
MM, Stationary 24 hrs	1500_D	180_D	135_D	165_D	1020_D			
	1367_C	61_C	132_C	147_C	1027_C	0.90	0.16	0.00
	1284_V	65_V	135_V	40_V	1044_V			
MM, Stationary 120 hrs	8100_D	170_D	130_D	2000_D	5800_D			
	7698_C	61_C	185_C	1173_C	6279_C	0.90	0.16	0.00
	6993_V	65_V	187_V	2077_V	4664_V			

Subscripts D = composite data, V = version *V*, and C = version *C*. Concentrations are in μM. Parameters: R_{HI}, 330 μM/hr; R_{LO}, 30 μM/hr; K_C, 30 μM; *cs*, 3; K_M, 115 μM; *ms*, 8. For version *C*, *px* = 1.4 and k_P = 0.034 hr^{-1}. For version *V*, *px* = 1.3 and k_P = 0.0006 hr^{-1}.